Using heat flux sensors for a contribution to experimental analysis of heat transfers on a triple-glazed supply-air window

Francois Gloriant, Annabelle Joulin, Pierre Tittelein, Stéphane Lassue

Version of Record: https://www.sciencedirect.com/science/article/pii/S0360544220322611
Manuscript_53c6605c19849b67eac5f7b50c40aa24

Using heat flux sensors for a contribution to experimental analysis of heat transfers on a triple-glazed supply-air window

François GLORIANT[1*], Annabelle JOULIN[2], Pierre TITTELEIN[2], Stéphane LASSUE[2]

[1]Laboratoire ICube (UMR-7357), Institut National des Sciences Appliquées de Strasbourg, 24 boulevard de la victoire, 67084 Strasbourg Cedex, France
[2]Laboratoire Génie Civil et géo-Environnement (EA-4515), Faculté des Sciences Appliquées - Université d'Artois, Technoparc Futura 62400 Béthune, France
[*](Corresponding author: francois.gloriant@insa-strabourg.fr)

Abstract – *An experimental set-up of triple-glazed supply-air window is developed in this research in order to characterize the window's thermal performance without solar radiation. By simultaneously measuring the local temperatures and heat fluxes with thermocouples and heat fluxmeters, the heat fluxes determination requires no longer using the correlations of heat transfer coefficients around the window, which are often the source of high uncertainties. Results show that the use of fluxmeters brought a more accurate measure of heat transfers around and in the window. Thereafter, the heat transfer coefficients can be correctly estimated by empirical evidence. Uncertainty analysis is then presented to highlight the reliability of the experimental method. Afterwards, the obtained experimental data are compared with those of numerical model developed by using Fluent® software. A thorough comparison analysis is provided to explain which parameters play a role in deviating the results between the two methods, leading to conclude the validity of numerical model assumptions with respect to the real conditions of experimental set-up.*

Keywords: *ventilated window; experimental prototype; heat fluxmeter; CFD; building ventilation*

Introduction

In recent buildings, smart windows may reduce heating and cooling costs while improving energy savings compared to conventional windows. Windows are a key component in a building and exert a major impact on building energy performance. Heat transfer coefficients have been regularly and sharply reduced over successive thermal regulations. These coefficients are however three or four times higher than the thermal coefficients of efficient opaque walls. Moreover, these windows significantly influence solar heat gain and incoming daylight, in contributing to the overall health and well-being of building occupants. Their implementation within the building envelope is especially delicate since windows are sensitive to heat loss through thermal bridges or airtightness defects.

To analyze the heating and cooling needs in a building, several studies have been conducted to characterize the thermal performance of windows and their influence on thermal comfort [1]. Many new technologies are now available. The double-glazed window is the most commonly used system in buildings, and its energy efficiency is typically improved through the use of a low-emission coating that reduces radiative heat losses [2]. The introduction of absorbent gases filling the gap between the glass panes had constituted an option for thermally efficient windows but has since become a standard feature [3]. Other authors have investigated the possibility of creating a partial vacuum between the panes, yet this approach would require installing spreaders to avoid pane deflection and bending [4].

On the other hand, many innovative systems are under investigation and offer the possibility of improving window energy efficiency. One technique calls for including different fin arrangements inside the gap in double-glazed windows in order to limit

convective movements and thus reduce heat transfer through the window [5]. Another innovative glazing system with an aerogel inclusion offers effective solutions for energy savings in winter, in addition to its utility in improving facade acoustics and lighting performance [6]. The ideal window should both preserve thermal comfort and utilize solar radiation as needed or else protect the building zone from overheating. These properties can be achieved thanks to thermotropic material-based windows, which change their light transmission behavior reversibly from transparent to turbid; they display a high performance when assessed in an indoor thermal environment, with energy and daylight under both hot summer and cold winter conditions [7]. These windows are currently very expensive and generate a slight reduction in light transmission and thus yield solar gains. High performance is also achievable with a double-glazed window featuring an inter-pane pleated cloth blind. This configuration influences flow structures in the air gaps by reducing the convective heat transfers between the glass panes [8].

Another improvement entails using the window to ensure the level of ventilation in buildings. Fresh air is not only drawn into the frame but circulates between the panes before reaching the indoor environment. This layout is called a "supply-air window". By circulating between the panes, the renewed fresh air modifies the heat losses between inside and outside and recovers a large share of the thermal flux. Preheated air then brings the calories back into the interior environment. In the context of retrofitting buildings [9], ventilated windows also offer the advantage of being easy to install.

The initial supply-air window patent was awarded to Morse [10]. The energy-related issue had not yet been a major concern; the main emphasis was to ensure effective building ventilation. Fish [11] then adopted the notion of optimizing the acoustic insulation of the air entrance. Another work, performed by Powell [12], sought to automate ventilation in the building. Ultimately, White's patent [13] showcased the supply-air window as a heat recovery device.

Several studies have highlighted the major thermal improvements compared to common double-glazed windows. The earliest studies on ventilated windows were conducted by Korkala [14] and Boehm [15]. Their results showed that this type of system tends to be a successful concept when used in individual housing. The preheated air significantly diminishes the heat consumption of a house in winter without degrading its thermal comfort. This performance is due to a lower temperature inside the window in the presence of airflow. Such a phenomenon leads to a drop in thermal losses heading towards the external environment.

The most frequently encountered case is the supply-air window with a double glazing on the internal side and a single facing on the outside [16–18]. A recent article [19] thoroughly investigated, both experimentally and numerically, the natural and forced convection as well as the thermal performance of a supply-air window. The set-up introduced was unique, with horizontal channels integrated at both the bottom and top of the frame for the injection and return of air through regularly-distributed perforations. More specifically, this work shows the benefit of a laminar flow rather than a turbulent regime for the energy performance optimization of the window. This article issued a recommendation of low-velocity flows. The model validation was essentially qualitative despite the extensive experiments implemented.

A supply-air window generally provides for air renewal from the outside into the building during winter. This concept is efficient whenever the thermal losses need to be reduced during the heating period. One possible solution consists of generating a satisfactory comfort level inside buildings along with lower energy consumption, for both cold winter climate when heating is required and warm summer climate when air conditioning is required. This solution

was proposed by Etzion and Erell [20]. The concept is based on a ventilated window designed with an absorptive glazing and a system that can easily rotate the window depending on the type of climate (external conditions). Air from the outside is drawn between the window panes and either enters the interior of the building in winter or directed back outside in summer.

The window studied in this work is a triple-glazed supply-air window, more specifically a Paziaud® window (Figure 1). This window was designed during the 1970's by Jacques Paziaud, French engineer and architect [21]. Its purpose is to ensure the preheating of the building's renewed air and consists of three glass planes delimiting a U-shaped channel through which air circulates [22,23]. The airflow inside this window is typically controlled by forced or mixed convection (at low velocity), associated with the building's air extraction system (mechanically or naturally assisted). The tests performed by the Paziaud Company in several refurbished houses with triple-glazed supply-air windows have revealed some interesting results. With regard to the airflow dynamics, the measured airflow rates are ranging from 8 to 15 $m^3.h^{-1}$ when the mechanical ventilation is activated, that remain relatively time-independent regardless of the climatic conditions (wind effet). Compared to the conventional air-inlet on the frame of window, the design of the U-shape channels in the novel triple-glazed supply-air window does not increase the pressure loss and does not lead to additional energy consumption of the mechanical fan. This is because the airflow in the window takes place at very low velocity (0.4 - 0.8 $m.s^{-1}$) in the laminar flow regime. As such, the additional pressure loss due to airflow between the panes is very small. In addition, the preheated air in the window creates buoyancy effects, thus increasing the airflow. The pressure loss will essentially occur in the window's air inlets (on both the exterior and interior frames), which are present in any kind of window (i.e. whether ventilated or not). In conclusion, the pressure loss due to airflow between the panes remains an insignificant problem.

With regard to the thermal performance of the window, the disposal is mainly interesting during winter conditions. The fresh air warms due to heat losses of the dwelling as well as a few solar radiations absorbed by the quasi-transparent glass panes. Note that the airflow rate features a decrease in the average window temperature when compared to a conventional triple-glazed window composed of the same elements (Figure 1). It gives rise, on the one hand, to a decrease in heat losses towards the external environment, while on the other hand to an increase in heat transfer between the window and the interior environment. This surplus heat flux stemming from the interior is "completely" recovered by the airflow. Lastly, when calculating an energy balance at the points of consumption (window and ventilation), the efficiency of the triple-glazed supply-air window is clearly higher than that of a classical system, such as a common window fitted with air vents [22,23].

This research has three main objectives :

The first objective is to compensate for a lack of experimental data on this type of window and to provide more experimental results in the realm of temperature and heat flux (data is provided here http://dx.doi.org/10.17632/n6b79v3d3y.1). Indeed, experimental studies performed in the past have mainly focused on windows with a single air cavity. The literature is short of experimental results regarding the triple-glazed supply-air window. In this research, the experimental set-up will be considered within a consistent range of airflow rates in order to evaluate the influence of airflow rate on the temperature and convective heat flux of the window.

The second objective is to propose an innovative experimental set-up. The use of heat fluxmeters contributes in large part to the originality of this experimental study. Their

application for opaque walls has already yielded satisfactory results in terms of accuracy, implementation and reliability [24]. For semi-transparent walls however, no experiments could be completed in our laboratory. The use of heat fluxmeters is relevant in this study for at least two following reasons:

- First, it provides direct measurement of heat fluxes, allowing to evaluate precisely the thermal performance of the window. As a matter of fact, the exclusive use of thermocouples does not permit to correctly estimate the thermal flux because the glass is a highly conductive material. The temperature difference between the faces of glazed-window is then too low to calculate precisely the crossed thermal flux. This phenomenon will be discussed in our present study. An experimental study conducted only by measure of thermocouples requires the use of correlations to deduce the heat transfer coefficient and consequently, to estimate the thermal flux. In our research, by using the heat fluxmeters, variation of thermal flux in different height and for each glass-pane will be highlighted.
- Secondly, the use of heat fluxmeters associated with thermocouples provides an experimental estimation of the heat transfer coefficients on both the outer and inner window parts. Indeed, the identification of heat transfer coefficients is a recurrent problem in building context. We will take a certain advantage from this experimental estimation of the heat transfer coefficients, by which the window's behavior may be more rigorously characterized, on the one hand, and numerical models can be more precisely calibrated, on the other hand. In this study, an empirical method to estimate the heat transfer coefficients will be proposed and the uncertainty of various parameters will be further discussed.

However, the studied experimental device has some limits. Unfortunately, it is not adapted to studying the effects of solar radiation. The installed fluxmeters are actually non-transparent. As such, in the presence of solar radiation, the fluxmeters would absorb a portion of this radiation, hence the measurement would be incorrect. Furthermore, it seems that a fluxmeter is sensitive to visible radiation, which is why we carried out our experimental campaign in the absence of light. Hence, this study will not address the thermal behavior of the window in the presence of solar radiation.

The third objective herein is to validate the numerical simulation model. This aspect is critical in allowing us to use the numerical results as references for assembling a "simplified" analytical model adapted to a building's thermal simulation [23]. Thereafter, use of this numerical model must enable carrying out parametric studies in order to accurately characterize the thermal performances of the disposed waste. By comparing the experimental results of this study to those of numerical simulations, this work will serve to highlight through experimentation the validity of assumptions employed in the numerical model. Consequently, this work will help to generate greater confidence in the numerical model.

1. Experimental design

1.1. The experimental set-up

The laboratory prototype was placed between two climate-controlled cells (Figure 2). The volume of each cell was approximately 12 m^3. The hot cell was equipped with two radiators while the cold cell was fitted with an air conditioner. The operative temperature was measured at the center of each cell with black globes and PT-100 temperature probes. Note that in this study, no significant difference between radiant temperature and ambient temperature was present. Since the cell walls were heavily insulated, the wall temperatures were very close to the air temperature. The deviation between these parameters was limited to the tenths of

degrees Celsius, thus corresponding to the predictable level of accuracy for measured temperatures.

To control the airflow rate inside the window, a convergent plenum [25] was installed at the top of the window (Figure 2). This plenum was needed to both avoid perturbations associated with the cell environment and gradually accumulate airflow inside a circular PVC pipe channel (diameter: 120 mm). A fan was required to vary the airflow rate inside the window. To measure this rate, an anemometer linked to a temperature probe was positioned upstream of the air fan at slightly more than 1.50 m from the plenum. In this study, the air intake and outlet had widths corresponding to the glass pane (w = 0.6 m) and were located under the upper frame. The air vents were typically no larger than the glass panes and installed on the window frame.

The triple-glazed supply-air window was equipped with thermocouples and heat flux sensors (Figure 3). The glass pane parameters are listed in Figure 3. The heat fluxmeters were placed both outside and inside the glass panes and distributed over a horizontal plane at three distinct height levels. The 0.1-mm diameter thermocouples were of type T [26] and provided a local measurement of pane wall and air temperatures. The 10 thermocouples used to measure air temperature were positioned at the center of each cavity by means of a stretched nylon wire. Some of the thermocouples were also placed at the channel entrance (T_{a0}) and exit (T_{a9}), as well as in the lower part of the junction between the two air cavities (T_{a4}). A high-precision thermistor sensor was also inserted outside both cells in order to determine the laboratory temperature. This thermistor served as a reference to calibrate all thermocouples before and during the experiment.

The fluxmetric sensors used were developed a few years ago in our laboratory [27–30]; they are qualified as "tangential gradient heat flux sensors" because their internal structure provides temperature gradients between thermoelectric junctions in the sensor plane. Their thickness is small (0.2 mm) for a 40-cm^2 (2 cm x 20 cm) sensor. The thinness of heat fluxmeters provides an advantage in that the heat flux measurement is not so intrusive. These fluxmeters feature a linear response for a temperature range between -20°C and +150°C; moreover, they can measure a heat flux from 0 to several kW/m^2. Since the window width equals 60 cm, the side effects are insignificant. Heat fluxmeters were stuck onto the glass. The glue layer presented no air bubbles (visible through the transparent material) and its thickness was negligible. Consequently, an excellent thermal contact with the glass could be obtained. None of the heat fluxmeters were placed on the low-emissivity window faces (= 0.17, data given by the manufacturer (see Figure 3) [31]).

Measurements were performed with a Keithley 2700 multimeter, and the data acquisition was automatically recorded on a computer by means of an IEEE-488 interface.

An initial set of experiments had been previously conducted [22,32], yielding the two following observations regarding the experimental set-up:

- The air conditioner generated undesirable air movements inside the cold room, particularly around the air inlet of the window. Consequently, to avoid this problem, it was decided not to use the air conditioning system in the cold room. Thanks to the wall inertia and insulation, the ambient temperatures were sufficiently constant to carry out measurements.
- Concerning thermal exchanges between the warm room and window, it was noted that the heat flux was smaller over the lower part of the window than over its upper part. This pattern could not be confirmed by the results obtained during the preliminary numerical studies [22,32]. Additional measurements indicated an air temperature stratification inside the hot cell. For an ambient temperature of 40.2°C, a 10°C difference was found

between the lower part of the window (34°C) and the upper part (44°C). A fan had to be installed in order to slightly move the air and produce a more homogeneous temperature inside this cell. With the fan, the temperature difference between window top and bottom dropped below 1.5°C. Note that the convective heat transfer coefficient in the warm room was modified by the fan.

Eight different airflow rates were compared (Table 1), corresponding to what could be measured in a common house, whether or not equipped with mechanical ventilation. The air temperature of the cold room was approx. 27°C. To generate a temperature differential of at least 20°C between the two cells for a measurable heat flux, the warm room temperature was set at 50°C. The temperature of the external environment remained constant at around 24°C during the tests. The result values for each sensor were averaged using over 100 measured points recorded at regular time intervals (20 or 30 seconds).

1.2. Analysis of measurement uncertainty

For each airflow rate, the data acquisition was recorded for a permanent flow when the temperatures of each cell were no longer fluctuating significantly. Figure 4 shows the experimental results for an airflow rate of 10.3 $m^3.h^{-1}$ (Test no. 3). Note that the laboratory temperature, at an average of 24.95°C, varied linearly from 24.88°C to 25.04°C during the 2-hour experiment. The temperatures in each cell were also very stable, varying within a range of 0.02°C in the cold cell and a range of 0.2°C in the warm cell. When changing the airflow rate, stabilization is obtained in less than an hour.

Measurements were recorded using a Keithley 2700 multimeter with a voltage resolution of 0.1 µV. The uncertainty due to multimeter resolution, i.e. about 0.6 µV, was negligible compared to that associated with the various sensors used in this experiment.

The 0.1-mm diameter thermocouples were of type T and exhibited an average sensitivity of approx. 39 $\mu V.°C^{-1}$ with an accuracy of ± 0.1°C [26]. The reference temperature at the cold junction was automatically measured by means of temperature sensors placed inside the multimeter. This compensation method at the cold junction was however not sufficiently precise for purposes of our study. For this reason, a T-type thermocouple was also associated with the high-precision thermistor sensor outside both cells. These sensors were glued together and installed in an insulated cell close to the multimeter. Such a set-up for measuring laboratory temperature introduces a systematic error of 0.1°C (Figure 4) and allows correcting the measurements of thermocouples placed inside the ventilated window.

The heat flux sensors, each covering a surface area of 40 cm², provide for an efficient sensitivity of roughly 20 $\mu V/(W.m^{-2})$ without any electrical supply. Depending on their positions, they generate a positive or negative voltage proportional to the heat flux across the sensor. Thanks to their low inertia, their response time is about one-tenth of a second. Their calibrations could be obtained by the "zero flux method" at 3% precision in our laboratory [33,34].

The heat fluxmeter to be calibrated was placed on a metal surface acting as a thermal sink. An electrical resistance of the same dimensions was positioned above the fluxmeter and enabled delivering a predetermined heat flux. To ensure having a full heat flux across the fluxmeter to be calibrated, no leakage was to be tolerated on the top layer of this set-up. For this reason, a second fluxmeter as well as a second heating resistance were positioned on the first resistance. This second fluxmeter was able to detect any heat leaks capable of being compensated by the second resistance controlled by a PID regulator. For a zero voltage at the terminals, the entire heat flux generated by the first resistance passed through the fluxmeter to

be calibrated. By varying the heat capacity of the first resistance, a calibration curve was plotted to determine the sensor sensitivity. Figure 5 shows this calibration curve for fluxmeter F_{61}. This result allows verifying the sensor response linearity within the measurement range of injected heating power. Note that the voltage response of this fluxmeter is proportional to the heat flux across it, with a sensitivity of 19.09 $\mu V/(W.m^{-2})$.

For each airflow tested, experimental results were obtained from an average of more than 100 recorded measurement values, hence reducing random errors. The statistical uncertainties shown in Figure 6 are nearly the same for all of the various airflow rates. Let's start by pointing out that the deviations in temperature measurements are small, with an uncertainty of less than 0.018°C for thermocouples placed both on the glass panes and inside the airflow. As regards the heat flux measurements, except for the heat fluxmeters on pane 3, the uncertainties lie below 1.0%. For fluxmeters F_{61}, F_{62} and F_{63}, uncertainties are greater yet still less than 2.0%. It can be expected that the measurements are noisy due to air movement generated by the presence of a fan in the warm room.

The random errors can thus be neglected in comparison with systematic errors due to the different measurement instruments. In the following part of the study, the uncertainties considered for each type of sensor are listed in Table 2; these uncertainties were increased in order to take into account the entire measurement system.

2. Experimental estimation of the heat transfer coefficients in the cells

The use of fluxmeters in this study is especially relevant. The experimental determination of heat flux from thermocouple measurements is unsatisfactory around the glass panes due to their lack of accuracy with respect to the high thermal conductivity of the glass. For Test no. 3 (Figure 4), the heat flux across the third glass, as calculated from the thermal resistance of the glass and with surface temperatures measured by the thermocouples, is unreasonably high and does not correspond to the data given by the heat fluxmeters, whose measurements (around 50-70 $W.m^{-2}$) are closer to reality. Moreover, other inconsistencies can be identified (Figure 4). The temperature difference between the two faces of a considered glazing is very small and sometimes contrasts with the direction of the corresponding measured heat flux. From the standpoint of measurement errors however, these temperature differences are acceptable, particularly for the low-emissivity coating surfaces. In these cases, the thermocouples are covered with a very thin, soft and adhesive aluminum sheet, which reveals the extent to which it is very difficult to measure the glass surface temperature. Taking into account these weak temperature differences and the high thermal conductivity of glass, the uncertainty is such that it would appear unreasonable to calculate heat flux from temperature measurements. In considering just the surface temperature uncertainties, the heat flux uncertainty value equals 71 $W.m^{-2}$ for the 4-mm thick glazing and 48 $W.m^{-2}$ for the 6-mm thickness. Heat fluxmeters are therefore a highly appreciated tool in the study of glazing.

The heat flux could be estimated inside the ambient rooms yet would have required prior knowledge of the heat transfer coefficients. From the normalized value defined in ISO 15099 [27] during the heating season, the interior convective heat transfer coefficient equals 3.6 $W.m^{-2}.°C^{-1}$. Since the experiments were performed without an air conditioner in the cold room, this value is acceptable for the cold cell. Regarding the warm cell, the presence of a fan generates airflow around the window at a velocity measured between 0.8 and 1 $m.s^{-1}$, which serves to increase the convective heat transfer. In respecting the correlation (Eq. 1) referenced in [35], the convective heat transfer coefficient in the hot cell can be estimated at approx. 8.5 $W.m^{-2}.°C^{-1}$.

$$h_c = 5.7 + 3.8\,W \qquad \textit{Eq. 1}$$

where W is the air velocity in ($m.s^{-1}$). This correlation is imprecise yet still provides an acceptable order of magnitude.

The radiative heat coefficient can be obtained by linearizing the heat transfer on gray surfaces (i.e. glass panes and cell walls):

$$h_r \approx 4\,\varepsilon\sigma T_m^3 \qquad \textit{Eq. 2}$$

where ε is the emissivity of the glazing and T_m the average temperature (in °K) between the glazing and the other cell surfaces: the result is roughly 6.3 $W.m^{-2}.°C^{-1}$ for the hot cell and 5.2 $W.m^{-2}.°C^{-1}$ for the cold cell. This output leads to global (convection and radiation) heat transfer coefficient values of 14.8 $W.m^{-2}.°C^{-1}$ for the hot cell and 8.8 $W.m^{-2}.°C^{-1}$ for the cold cell.

A major benefit of this study lies in the experimental determination of the global heat transfer coefficients based on heat flux and temperature data without having to rely on the previous correlations.

The heat transfer coefficient h_2 is calculated from sensor measurements recorded on the 6th wall of the window as well as with the PT-100 sensor in the warm cell. The sensors placed at three different levels provide three estimations of h_2 (Eq. 3). The heat transfer coefficient in the cold cell h_1 can be determined in four separate ways. Its value may be calculated from sensors placed at mid-height of the 1st wall of the window, while it is also possible to calculate this coefficient from sensors located on the 2nd wall of the window, although in this case, the thermal resistivity of the 1st wall should be taken into account.

$$h_{2j} = \frac{\varphi_{6j}}{\theta_2 - \theta_{6j}} \text{ with } \; j = \{1, 2, 3\} \qquad \textit{Eq. 3}$$

$$h_{10} = \frac{\varphi_{12}}{\theta_{12} - \theta_1} \qquad \textit{Eq. 4}$$

$$h_{1j} = \left(\frac{\theta_{2j} - \theta_{cc}}{\varphi_{2j}} - \frac{e}{\lambda}\right)^{-1} \text{ with } \; j = \{1, 2, 3\} \qquad \textit{Eq. 5}$$

The determination of uncertainty for the heat transfer coefficient estimation is based on the Kline and McClintock method [36], as follows:

$$\omega_h = \left(\left(\frac{\partial h}{\partial \varphi}\omega_f\right)^2 + \left(\frac{\partial h}{\partial \theta_{pt}}\omega_{pt}\right)^2 + \left(\frac{\partial h}{\partial \theta_{th}}\omega_{th}\right)^2\right)^{0.5} \qquad \textit{Eq. 6}$$

The uncertainties for the heat flux and temperature measurements are listed in Table 2. Note that in this equation (Eq. 5), the uncertainty of the glass thermal resistivity has been neglected because this resistance (approx. 0.004 $K.m^2.W^{-1}$) is very low compared to the heat flux coefficient. The heat flux coefficient results for each cell are depicted in Figure 7 and 8, according to both the sensor location and test under consideration.

As for the estimation of the coefficient h_2 in the warm cell (Figure 8), the results are satisfactory. The relative error of the overall estimation equals about 8%; this finding is mainly due to the inaccuracy of fluxmeters and thermocouples. Note that these results are stable and do not vary from one test to the next. However, the estimations differ depending on sensor location. The average values for the 8 tests are: 12.9 ± 0.8 $W.m^{-2}.°C^{-1}$ at the bottom of the window, 14.6 ± 1.0 $W.m^{-2}.°C^{-1}$ at mid-height, and 15.9 ± 1.2 $W.m^{-2}.°C^{-1}$ at the top.

This phenomenon may be due to measurement inaccuracy; however, this would not be the principal reason. As mentioned above, despite the presence of a fan in the warm cell, a vertical temperature gradient still remains between the bottom and top of the window, estimated at 1.5°C. As an initial approximation, this phenomenon can be taken into account by assuming a linear behavior of the ambient temperature, increased by 0.4°C for the 0.75 *H* level and decreased by 0.4°C for the 0.25 *H* level. The results are more homogeneous, with an average value for the 8 tests of: 13.8 ± 0.8 $W.m^{-2}.°C^{-1}$ at the bottom, 14.6 ± 1.0 $W.m^{-2}.°C^{-1}$ at mid-height, and 14.3 ± 1.2 $W.m^{-2}.°C^{-1}$ at the top. One should bear in mind that for the remainder of this study, the ambient temperature variation with respect to window height has not been taken into account. The heat transfer coefficient magnitude in the warm cell was set at 14.6 $W.m^{-2}.°C^{-1}$, as estimated at mid-height of the window. Also note that this value lies close to that obtained from the previous correlations.

As regards estimation of the coefficient h_1 in the cold cell (Figure 7), results are also satisfactory for the first three tests. The average value for these 3 experiments and 4 measurement positions is: 7.7 ± 0.8 $W.m^{-2}.°C^{-1}$. The relative error is approx. 10%, i.e. slightly higher than that obtained for coefficient h_2 in the warm cell. As of the 4th test, the uncertainties increase, particularly for measurements at the top of the window. This phenomenon is due to the window temperature, which decreases as airflow rate increases. The heat flux between window and cell, as well as the temperature difference between glazing and air inside the cell, becomes too low, thus generating an increase in measurement uncertainty. Let's point out here that thermocouple inaccuracy is the main reason preventing a good estimation of h_1 at high airflow rates. For the remainder of this study, the value of coefficient h_1 was set at 7.7 $W.m^{-2}.°C^{-1}$, with this estimation being slightly lower than that output by the correlations.

3. Numerical simulations

3.1. Modeling approach

A numerical work has studied a 2D laminar steady-state airflow, driven by mixed convection, occurring in a triple-glazed supply-air window (Figure 9). The ISO 15099 Standard served to determine the temperature-dependent thermophysical properties of the fluid. Fluid properties followed polynomial functions, and the incompressible ideal gas law was applied to take density variation into account [37]. The governing equations were solved with the commercial CFD software Fluent® [38], based on the finite volume method with a pressure-based solver (Figure 9). The momentum and pressure-based continuity equations were solved simultaneously with the coupled algorithm. The radiation model applied to solve the longwave radiative transfer was the Discrete Ordinates (DO) radiation model [39]. Convergence criteria were set at 10^{-6} for continuity, 10^{-8} for energy and 10^{-8} for velocity and radiation.

A non-uniform structured grid composed of 79,200 cells, refined near the glass panes and the inlet and outlet, was selected for this study (Figure 9). A grid sensitivity analysis was conducted to ensure the adequacy of this mesh density beforehand [22], by comparing 3 different structured grids of 73,200, 99,200 and 292,800 cells, respectively (Figure 10). It has been done with thermal conditions according to the ISO 15099 Standard [37] for an airflow of 20 $m^3.h^{-1}$. It was shown that the flux and temperature results were very similar for all 3 grids, with a maximum difference of 0.1°C for temperature and 0.5 $W.m^{-2}$ for flux. The complete study can be found in the first author's phD thesis [22].

3.2. Boundary conditions of the CFD model

To compare results from the experimental device and from numerical simulations, the boundary conditions introduced in the numerical model had to be consistent with the window environment (Figure 9).

At the entrance, air temperature corresponds to the measured experimental value θ_{a0}. An airflow rate identical to that measured by the anemometer was also set on this boundary, in considering the air density variation.

The external boundary conditions for glass panes 1 and 3 are Fourier boundary conditions (third type). The ambient reference temperature for each wall corresponds to the temperature measured in the considered cell. For the radiative heat flux, as explained above, the average air temperature of the cell walls nearly equaled the resultant temperature (maximum deviation: 0.1°C).

4. Comparison of numerical and experimental results

4.1. Analysis of surface temperatures and heat fluxes

Temperature estimations from the numerical simulations were in line with experimental data (Figures 11, 12, 13 and 14). The wall temperature differences were limited. The average difference between measurement and simulation over all 18 measurement positions and among the 8 tests conducted was 0.44°C. The largest difference was observed for thermocouple T_{42} during Test 5: 1.28°C. It can be remarked that the most predominant differences were observed around the second glass pane, with an average difference of 0.67°C, compared to 0.34°C and 0.31°C for the first and third panes, respectively. Except for this singular observation, the differences between numerical and experimental data specific to surface temperature cannot be ascribed to the presence of a low-emissivity surface, or to volume airflow variation or to sensor positions in the window. In general, it would seem that the numerical model tends to underestimate surface temperatures.

Concerning the heat flux determinations, results here (see Figures 15 and 16) clearly demonstrate a good match for each glazing between numerical and experimental data. As expected, the greater the heat flux, the smaller the difference between numerical and experimental output. The sensors on the third glass pane display an average difference of 3%, while those on the second glass differ by 15% and those on the first by 31%.

Heat fluxes for glazing 1 are weak and become increasingly weaker with airflow rate. The relative difference reaches above 60% during Test 8 on this glass. In taking into account the systematic error of a heat flux sensor (about 1 $W.m^{-2}$), it is difficult to draw a conclusion regarding heat flux measurements of the window on this side.

Over all 8 tests, the mean difference equals 2.8 $W.m^{-2}$. This value varies quite little with airflow. As for surface temperatures, differences are highest around the second glass pane (3.4 $W.m^{-2}$ on average vs. 2.2 $W.m^{-2}$ for the first and 2.0 $W.m^{-2}$ for the third). For glass panes 1 and 2, the model tends to underestimate heat flux yet it remains in the high zone for the second cavity, where this underestimation is the most pronounced. The vicinity of fluxmeter F_{43} produces by far the highest differences. The maximum difference, reached during Test 8, equals 8.1 $W.m^{-2}$. The lower the airflow, the smaller this difference. In considering all 8 tests, the average relative difference is therefore reduced to 5.6 $W.m^{-2}$. Airflow thus exerts an influence in this zone. The influence being exerted close to fluxmeter F_{42} is also substantial but less significant.

4.2. Analysis of air temperature in the air layers

As regards air temperature, the comparison between numerical and experimental data is more nuanced. The results remain consistent even though the deviation widens (Figures 12 and 13). As for surface temperature, the numerical model tends to underestimate air temperature, and this deviation increases with airflow rate. However, a better similarity between results can be noticed nearer the outlet of each cavity (Figure 14). To understand and explain these differences, it is necessary to accurately identify the subject of comparison. In numerical simulations, the air temperature determination corresponds to the bulk temperature. In an experimental set-up on the other hand, air temperature is determined by means of thermocouples T_{ak} suspended in the cavities. The air temperature measurement in low-thickness cavities is difficult to perform with thermocouples, and it would be fair to question what is actually being measured by the sensors; it is clear that these are not local measurements of air on the thickness between glass panes because even if the thermocouples used in this experiment are thin (0.2 mm max), measuring in the window cavities is unavoidably intrusive, and radiative heat transfer can have little effect on the measurement result. The presence of a thermocouple modifies streamlines and generates local turbulence in the air. This phenomenon tends to increase mixing and heat transfer. Air temperatures become higher and more homogeneous within the cavity section containing the thermocouples. The fact that the numerical model fails to consider these obstacles leads to an underestimation of air temperature in the primary parts of each cavity. As air velocity increases, local air turbulence increases around thermocouples and temperature differences between the panes widen, thus contributing to a greater deviation between experimental and numerical data. As regards the cavity outlet however, air turbulence is not only due to the presence of thermocouples T_{a4}, T_{a8} and T_{a9} but above all stems from flow direction changes. The numerical model considers these singularities, which is why differences are smaller between experimental and numerical output (Figure 14).

For air temperature in the first cavity, the average difference over the 8-test campaign is 0.36°C, which is almost within the thermocouple margin of error (±0.29°C). Regarding the second cavity, the temperature rise is experimentally determined by two methods using either thermocouples T_{a4} and T_{a8} or thermocouples T_{a4} and T_{a9}. For Tests 1 through 4, the temperature rise in the second cavity estimated with sensors T_{a4} and T_{a9} lies closer to the numerical result than the estimation with T_{a4} and T_{a8}. From these 4 tests, the difference between experimental and numerical results is thus 0.22°C based on T_{a4} and T_{a9} and 0.60°C based on T_{a4} and T_{a8}. On the other hand, for Tests 5 through 8, temperature estimations based on T_{a4} and T_{a8} yield better numerical estimations. The difference between experimental and numerical data amounts to 0.98°C based on T_{a4} and T_{a9}, while it is reduced to 0.18°C based on T_{a4} and T_{a8}. Thermocouples T_{a8} and T_{a9} are separated by just a few centimeters and yet, as the airflow rate increases, the difference between these two sensor measurement increases. This phenomenon can be explained by locally analyzing streamlines around the window outlet. In this study, any identification requires running the numerical model. Let's note that close to the outlet, a recirculation zone occurs, where a trickle of exterior air penetrates into the window before being discharged by the main flow and exiting. This phenomenon becomes even more pronounced at high airflow rates. This trickle of hot air thus tends to increase temperature in the zone around thermocouple T_{a9}. Numerical simulation has been able to predict this phenomenon for the window instrumentation herein, which is why thermocouple T_{a8} was added slightly upstream of thermocouple T_{a9}, to ensure restricting the influence on outlet temperature estimation in the second cavity by this air recirculation when the airflow rate becomes excessive.

4.3. Discussion on modeling assumptions

The results of this experimental study confirm the assumptions inherent in the numerical model. The triple-glazed supply-air window may be modeled in its current state as a semi-transparent ventilated window, in considering bidimensional geometry and a laminar flow. The mesh composed of some 73,200 cells seems to be adequately refined to obtain accurate results. The experimental estimation of heat transfer coefficients close to the glass panes plays an important role in building a numerical model most closely matching experimental conditions.

However, the differences between experimental and numerical data observed on pane 2 cannot be ascribed solely to a lack of sensor precision. The numerical model obviously underestimates the heat flux and temperatures on this pane. This phenomenon may be explained in two potentially interdependent ways. First of all, when a thermal balance is assessed on the window, notably for a high airflow rate, a lack of heat flow becomes readily apparent. Indeed, while the numerical and experimental data agree on inlet and outlet heat fluxes on the first and third panes as well as on the heat flux renewed by air, how then can the numerical underestimation close to the second glass be explained? The heat flux stemming from the window frame, which is neglected in the numerical model, should be taken into account particularly when the airflow is considerable. As airflow increases, the air temperature inside the window is cooling, thus generating greater heat suction at the window frame. The hypothesis of an adiabatic wall for the window frame is therefore undoubtedly more questionable in this study. Moreover, if this hypothesis is not made, then the heat transfer across the frame would introduce an asymmetry that could only be considered by a three-dimensional representation of the window. Secondly, the turbulent structures amplifying preheating of the air might not be correctly depicted. The assumption of laminar flow in some parts of the window needs to be questioned at high airflow rates.

At this stage, no criteria have been established to determine the type of flow regime inside a supply-air window. For example, Kim *et al.* [40,41] forwarded the assumption of laminar flow with a Reynolds number of less than 1,500. Opinions are divided however regarding the flow regime. In most cases [16–18,42–46], the possible presence of a turbulent phenomenon has been neglected. In contrast, some studies [19,47,48] have proposed taking a turbulent flow into account, but only Bhamjee [19] has experimentally observed turbulent phenomena at the cavity entrance. In any event, research findings have converged on one specific point highlighted by Tjelflaat [49]: a smooth laminar airflow leads to the best compromise between preheating and thermal insulation. In a turbulent regime, the air-wall exchanges are emphasized, thus generating a greater preheating of air, but also increased thermal losses. Maintaining a laminar flow thus seems necessary in order to ensure optimal thermal insulation. This observation has also been confirmed by our experimental set-up, in which the presence of thermocouples in the middle of cavities apparently increases thermal exchanges.

As regards the type of thermal exchanges taking place in the cavities, a mixed or forced convection could be expected. Experimental data do not allow drawing a direct conclusion on this question. However, the numerical model that has just been validated clearly shows that the velocity profile in the main part of the window is parabolic. Nevertheless, let's underscore here that a slight asymmetry is observed for the two first tests when the airflow rate is less than 8 $m^3.h^{-1}$. Additional simulations also indicate that the temperature difference on both sides of the window exerts no influence on the airflow dynamic. It would seem that convection is being forced on the airflow rate range tested herein, removing the necessity to consider the variation in the thermophysical properties of air. This conclusion is due to the air cavity thickness (less than 2 cm) and would no longer be applicable for larger cavities.

Airflow is much more variable versus time and strongly depends on both the climate [43] [50] and window geometry [51].

4.4. Discussion on performance of the triple-glazed supply-air window

In the absence of a solar heat flux, the benefit of this experimental set-up lies in minimizing heat flux between the window and the external environment via a controlled airflow. As an initial result, the greater the airflow, the closer the temperature of the external environment lies to the mean window air temperature. Consequently, the effect is a decrease in thermal losses through the window. From a thermal comfort standpoint however, it is still necessary for the airflow rate to remain not too high in order to maintain a comfortable temperature on the glass panes for the interior environment or at the window outlet. A compromise thus must be found between heat loss and thermal comfort.

Numerical and experimental results are in good agreement regarding the following considerations:

- The air does not recover a large share of the heat in the first cavity. The behavior of air temperature is characterized by an increase at the higher window level and a decrease over the lower part of the window. This phenomenon is increasingly less sensitive as the airflow rate increases.
- Preheating of the incoming air essentially takes place in the second cavity.
- The temperature difference between walls is small in the first cavity, in comparison with the second cavity. This phenomenon becomes more sensitive as the airflow rate increases.
- As the airflow rate increases, air temperature drops at the window outlet, with the heat flux increasing between the window and the warm atmosphere and decreasing between the window and the cold room.
- For low airflow rates, a slight decrease in air temperature can be observed at the upper level of the second cavity. This phenomenon does not occur in the experiments at higher airflow rates.

Conclusion

This article presents an experimental study aiming to characterize the thermal behavior of a triple-glazed supply-air window in steady state condition without solar radiation. Installed between two climate-controlled cells and instrumented with thermocouples and fluxmeters, the device was subjected to different air flows ranging from 5 to 30 $m^3.h^{-1}$. The use of fluxmeters has proved to be very relevant and formed the main originality of this work.

Firstly, the fluxmeters allow direct measurement of heat transfer around and in the window with 5% of accuracy. Without those instruments, it is not possible to achieve such precision. Indeed, the theoretical heat flux estimation method by using the thermal resistance of the glass and the measured surface temperatures would lead to an uncertainty greater than 50%. The reliability of heat fluxmeters and thermocouples for surface measurements provides then a precise mapping of the window's thermal behavior for a given flow. However, the air temperatures measurement in the window cavities remain difficult to perform because it is unavoidably intrusive.

Secondly, the use of heat fluxmeters associated with thermocouples allows giving an empirical estimation of the heat transfer coefficients in each cell. The identification of heat transfer coefficients is a recurrent problem in building context and the use of existing correlations is often necessary. Over all experimental tests, it is shown that the experimental heat transfer coefficient results are stable for each cell with a relative error of about 8%.

Finally, the direct measurement of heat flux and the experimental estimation of heat transfer coefficients helps to build the most corresponding numerical model to the experimental conditions. The results of the two methods show only slight difference: 0.44°C for the surface temperatures and 2.8 $W.m^{-2}$ for the heat flux. The experimental set-up has then proven the relevance of numerical modeling and its main hypotheses: the triple-glazed supply-air window may be modeled in its current state as a semi-transparent ventilated window by considering bidimensional geometry and a laminar flow.

Acknowledgements

This research is financed thanks to the European program INTERREG IV – Innovation FOr REnewal (IFORE) project.

Nomenclature

CFD	Computational Fluid Dynamics
e	glass thickness, m
exp	experimentations
F_{ij}	heat fluxmeter of the pane of glass i at the position j
H	window height, m
h	global heat transfer coefficient, $W.m^{-2}.°C^{-1}$
h_1	global heat transfer coefficient in the cold cell (cell n°1), $W.m^{-2}.°C^{-1}$
h_2	global heat transfer coefficient in the hot cell (cell n°2), $W.m^{-2}.°C^{-1}$
h_c	convective heat transfer coefficient, $W.m^{-2}.°C^{-1}$
h_r	radiative heat transfer coefficient, $W.m^{-2}.°C^{-1}$
l	window width, m
P_{atm}	atmospheric pression, Pa
T_1	PT-100 temperature probe in the cold cell (cell n°1)
T_2	PT-100 temperature probe in the hot cell (cell n°2)
T_{ak}	thermocouple in the air channel at the position k, °C
T_{ij}	thermocouple of the pane of glass i at the position j
V	volumetric airflow rate, $m^3.h^{-1}$
W	mean air velocity, $m.s^{-1}$

Greek symbols:

ΔP	pressure difference between the inlet and the outlet of the window, Pa
ε	emissivity of the pane of glass
θ_1	air temperature measure in the cold cell (cell n°1), °C
θ_2	air temperature measure in the hot cell (cell n°2), °C
θ_{ak}	air temperature measure at the position k, °C
θ_{CFD}	temperature estimation by simulation, °C
θ_{ij}	temperature measure at the pane of glass i at the position j, °C
θ_{pt}	temperature measure by a PT-100 sensor, °C
θ_{th}	temperature measure by a thermocouple sensor, °C
λ	thermal conductivity of the glass, $W.m^{-1}.°C^{-1}$
σ	Stefan-Boltzmann constant, $W.m^{-2}.K^{-4}$
φ	heat flux measure, $W.m^{-2}$
φ_{CFD}	heat flux estimation by simulation, $W.m^{-2}$
φ_{ij}	heat flux measure at the pane of glass i at the position j, $W.m^{-2}$
ω_a	uncertainty on the airflow rate measurement, $m^3.s^{-1}$
ω_f	uncertainty on the heat flux measurement, $W.m^{-2}$
ω_h	uncertainty on the heat transfer coefficient measurement, $W.m^{-2}.°C^{-1}$
ω_{pt}	uncertainty on the temperature measurement by PT-100 sensor, °C
ω_{th}	uncertainty on the temperature measurement by thermocouple, $m^3.s^{-1}$

References

[1] Cappelletti F, Prada A, Romagnoni P, Gasparella A. Passive performance of glazed components in heating and cooling of an open-space office under controlled indoor thermal comfort. Build Environ 2014;72:131–44. http://dx.doi.org/10.1016/j.buildenv.2013.10.022.

[2] Mohelnikova J. Materials for reflective coatings of window glass applications. Constr Build Mater 2009;23:1993–8. http://dx.doi.org/10.1016/j.conbuildmat.2008.08.033.

[3] Ismail KAR, Salinas CT, Henriquez JR. A comparative study of naturally ventilated and gas filled windows for hot climates. Energy Convers Manag 2009;50:1691–1703. https://doi.org/10.1016/j.enconman.2009.03.026.

[4] Sullivan R, Beck FA, Arasteh DK, Selkowitz SE. Energy performance of evacuated glazings in residential buildings. Trans-Am Soc Heat Refrig AIR Cond Eng 1996;102:220–227.

[5] Giorgi LD, Bertola V, Cafaro E. Thermal convection in double glazed windows with structured gap. Energy Build 2011;43:2034–8. http://dx.doi.org/10.1016/j.enbuild.2011.03.043.

[6] Cotana F, Pisello AL, Moretti E, Buratti C. Multipurpose characterization of glazing systems with silica aerogel: In-field experimental analysis of thermal-energy, lighting and acoustic performance. Build Environ 2014;81:92–102. https://doi.org/10.1016/j.buildenv.2014.06.014.

[7] Yao J, Zhu N. Evaluation of indoor thermal environmental, energy and daylighting performance of thermotropic windows. Build Environ 2012;49:283–90. http://dx.doi.org/10.1016/j.buildenv.2011.06.004.

[8] Dalal R, Naylor D, Roeleveld D. A {CFD} study of convection in a double glazed window with an enclosed pleated blind. Energy Build 2009;41:1256–62. http://dx.doi.org/10.1016/j.enbuild.2009.07.024.

[9] Sdei A, Gloriant F, Tittelein P, Lassue S, Hanna P, Beslay C, et al. Social housing retrofit strategies in England and France: A parametric and behavioural analysis. Energy Res Soc Sci 2015;10:62–71. http://dx.doi.org/10.1016/j.erss.2015.07.001.

[10] Morse ES. Warming and ventilating apartments by the sun's rays. 246626, n.d.

[11] Fisk ET. Sound excluding ventilating window. 2125669, n.d.

[12] Powell GA. Automatic ventilator window. 3034416, n.d.

[13] White WS. Heat exchanger window. 3925945, n.d.

[14] Korkala T, Saarnio P, Siitonen V. Air intake arrangements of the supply air window from the view of comfort and ventilation efficiency. Proceeeding Window Build., Sweden: 1984.

[15] Boehm RF, Brandle K. Testing of air-flow windows for evaluation and application. Sol. Energy Conf., Reno, Nevada, USA: 1980.

[16] Baker PH, McEvoy ME. Test cell analysis of the use of a supply air window as a passive solar component. Sol Energy 2000;69:113–130. https://doi.org/10.1016/S0038-092X(00)00048-7.

[17] McEvoy ME, Southall RG, Baker PH. Test cell evaluation of supply air windows to characterise their optimum performance and its verification by the use of modelling

techniques. Energy Build 2003;35:1009–1020. https://doi.org/10.1016/S0378-7788(03)00042-2.

[18] Southall RG, McEvoy ME. Investigations into the functioning of a supply air window in relation to solar energy as determined by experiment and simulation. Sol Energy 2006;80:512–523. https://doi.org/10.1016/j.solener.2005.04.016.

[19] Bhamjee M, Nurick A, Madyira DM. An experimentally validated mathematical and CFD model of a supply air window: Forced and natural flow. Energy Build 2013;57:289–301. https://doi.org/10.1016/j.enbuild.2012.10.043.

[20] Etzion Y, Erell E. Controlling the transmission of radiant energy through windows: a novel ventilated reversible glazing system. Build Environ 2000;35:433–44. http://dx.doi.org/10.1016/S0360-1323(99)00039-6.

[21] Paziaud J. Fenêtre à isolation dynamique par circulation d'air. 8205279, n.d.

[22] Gloriant F. Caractérisation et modélisation d'une fenêtre pariéto-dynamique à trois vitrages. doctorat. Université d'Artois, 2014.

[23] Gloriant F, Tittelein P, Joulin A, Lassue S. Modeling a triple-glazed supply-air window. Build Environ 2015;84:1–9. http://dx.doi.org/10.1016/j.buildenv.2014.10.017.

[24] Lassue S, Güths S, Leclercq D, Duthoit B. Contribution to the experimental study of natural convection by heat flux measurement and anemometry using thermoelectric effects. Exp Heat Transf Fluid Mech Thermodyn 1993:831–8.

[25] CSTB. Rapport d'essais n°35078. 1995.

[26] Nau M. Mesure électrique de la température: avec des thermocouples et des sondes à résistance. Juchheim; 2003.

[27] Thureau P. Fluxmètres thermiques. Tech Ing Mes Gd Thermophysiques 2015;base documentaire : TIB544DUO.

[28] Herin P, Thery P. Measurements on the thermoelectric properties of thin layers of two metals in electrical contact. Application for designing new heat-flow sensors. Meas Sci Technol 1992;3:495.

[29] Leclercq D, Thery P. Apparatus for simultaneous temperature and heat-flow measurements under transient conditions. Rev Sci Instrum 1983;54:374–80. http://dx.doi.org/10.1063/1.1137377.

[30] Devisme J-M, Langlet T, Douzane O, Roucoult J-M, Quéneudec M. Étude théorique et expérimentale de fluxmètres à "gradient transversal" pour la thermique du bâtiment. Int J Therm Sci 2001;40:205–15. http://dx.doi.org/10.1016/S1290-0729(00)01209-6.

[31] Tarcog (Carli, Inc.). TARCOG : Mathematical models for calculation of thermal performance of glazing systems with or without shading devices. 2006.

[32] Gloriant F, Tittelein P, Joulin A, Lassue S. Etude expérimentale d'une fenêtre parieto-dynamique de type Paziaud®, La Rochelle (France): 2015.

[33] Güths S. Anémomètre à effet Peltier et fluxmètre thermique: conception et réalisation, application à l'étude de la convection naturelle. 1994.

[34] Oter LD. Application des méthodes de la théorie des systèmes à la simulation de l'évolution des flux thermiques sur les faces d'entrée et de sortie d'une paroi multicouche. 1985.

[35] MacAdams WH. Heat transmission. New York: McGraw-Hill; 1954.

[36] Kline SJ, McClintock FA. Describing Uncertainties in Single-Sample Experiments. Mech Eng 1953:3–8.

[37] ISO. Thermal performance of windows, doors and shading devices - detailed calculations. 2003.

[38] Fluent. UG, Fluent Inc, Fluent 6.3 User's Guide, Lebanon, NH 2006.

[39] Fiveland W. Discrete-ordinates solutions of the radiative transport equation for rectangular enclosures. J Heat Transf 1984;106:699–706.

[40] Kim M-H, Oh C-Y, Hwang J-H, Choi H-W, Yang W-J. Thermal performance of the exhausting and the semi-exhausting triple-glazed airflow windows. Int J Energy Res 2006;30:177–190. https://doi.org/10.1002/er.1149.

[41] Kim M-H, Yang W-J. An optimum design on the triple-glazed exhaust airflow window. Int J Energy Res 2002;26:355–364. https://doi.org/10.1002/er.789.

[42] Carlos JS, Corvacho H. Evaluation of the thermal performance indices of a ventilated double window through experimental and analytical procedures: Uw-values. Renew Energy 2014;63:747–54. https://doi.org/10.1016/j.renene.2013.10.031.

[43] Carlos JS, Corvacho H, Silva PD, Castro-Gomes JP. Modelling and simulation of a ventilated double window. Appl Therm Eng 2011;31:93–102. https://doi.org/10.1016/j.applthermaleng.2010.08.021.

[44] Wei J, Zhao J, Chen Q. Energy performance of a dual airflow window under different climates. Energy Build 2010;42:111–122. https://doi.org/10.1016/j.enbuild.2009.07.018.

[45] Wei J, Zhao J, Chen Q. Optimal design for a dual-airflow window for different climate regions in China. Energy Build 2010;42:2200–2205. https://doi.org/10.1016/j.enbuild.2010.07.016.

[46] Wright JL. Effective U-values and shading coefficients of preheat/supply air glazing systems. Proc Sol. Energy Soc. Can., Winnipeg, Canada: 1986, p. 219–24.

[47] Gosselin JR, Chen Q (Yan). A computational method for calculating heat transfer and airflow through a dual-airflow window. Energy Build 2008;40:452–458. https://doi.org/10.1016/j.enbuild.2007.03.010.

[48] Raffnsøe LM. Thermal Performance of Air Flow Windows. Master Thesis. Danmarks Tesniske Universitet, 2007.

[49] Tjelflaat PO, Bergensen B. Improved thermal insulation in windows by laminar air flows. Therm Perform Exter Envel Build III 1985.

[50] Carlos JS, Corvacho H, Silva PD, Castro-Gomes JP. Real climate experimental study of two double window systems with preheating of ventilation air. Energy Build 2010;42:928–934. https://doi.org/10.1016/j.enbuild.2010.01.003.

[51] Ismail KAR, Henríquez JR. Two-dimensional model for the double glass naturally ventilated window. Int J Heat Mass Transf 2005;48:461–475. https://doi.org/10.1016/j.ijheatmasstransfer.2004.09.022.

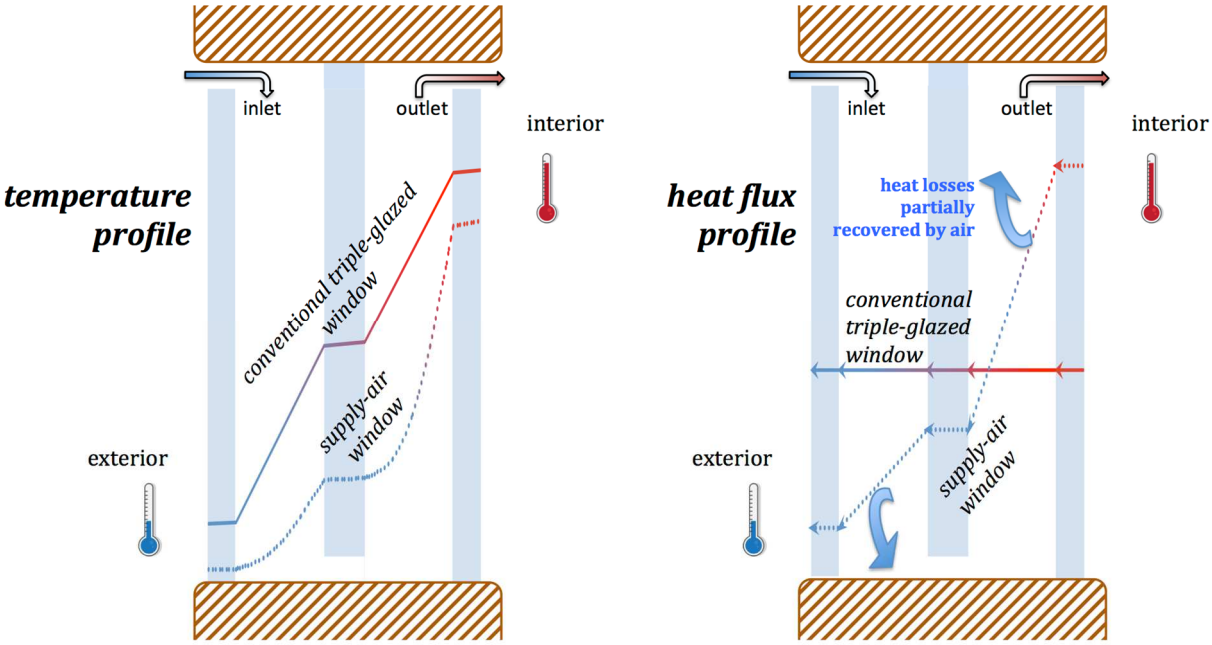

Figure 1: Operating principle of a supply-air window during the heating season

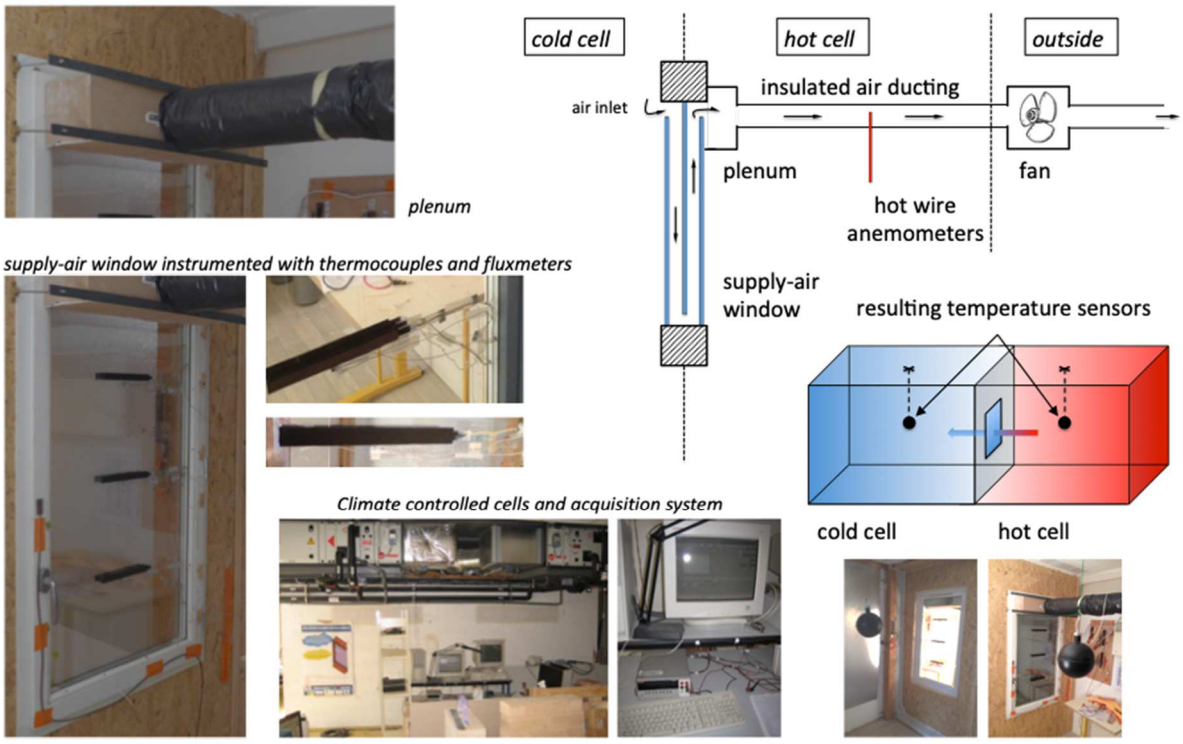

Figure 2: Experimental set-up

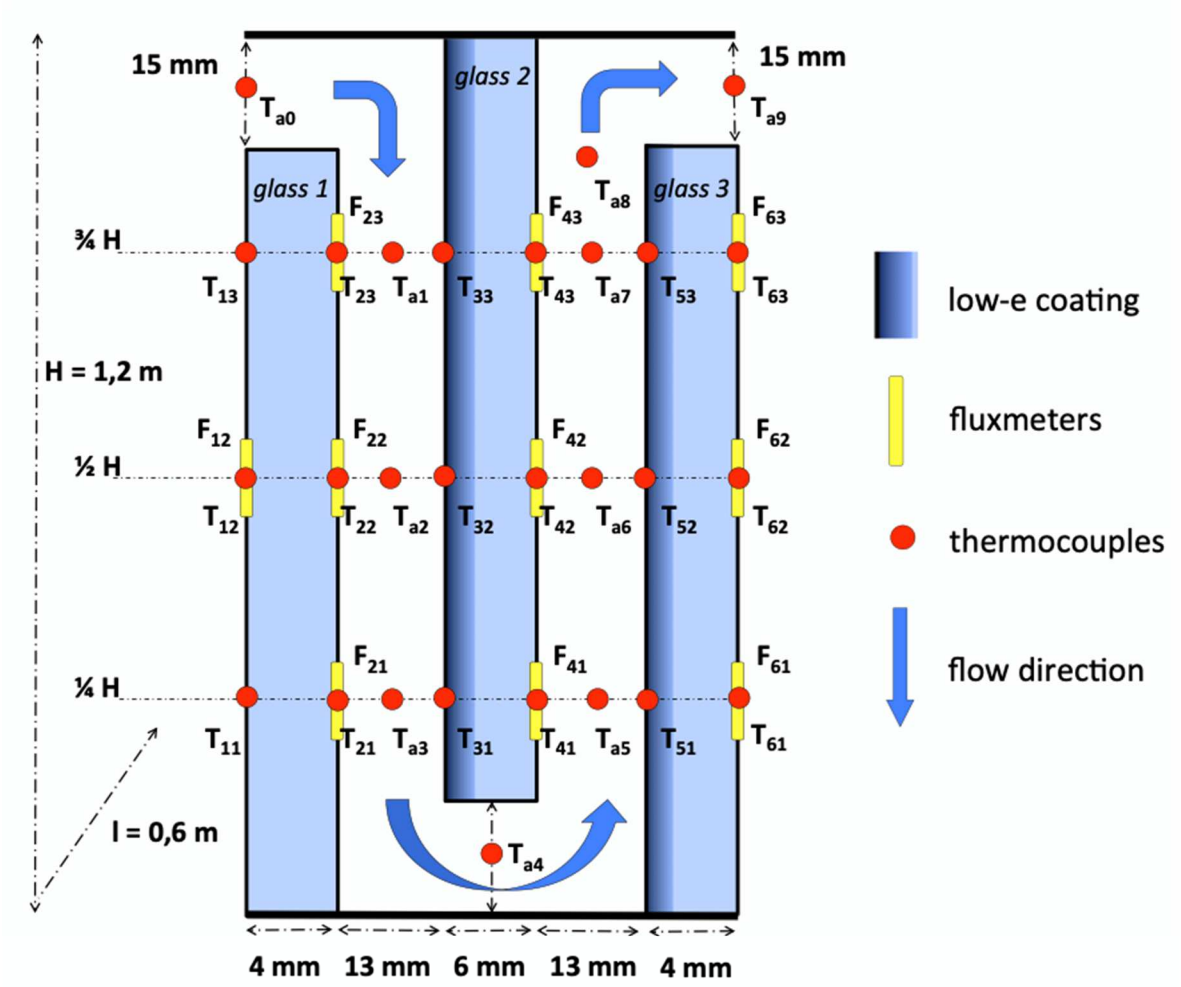

	Glass 1	Glass 2	Glass 3
Manufacturer's reference	4 mm Planibel® Clearvision	6 mm Planibel G® pos.2	4 mm Planibel G® pos.2
Emissivity of the glass surface	0.84 / 0.84	0.17 / 0.84	0.17 / 0.84

Figure 3: Instrumentation and radiation parameters of the supply-air window

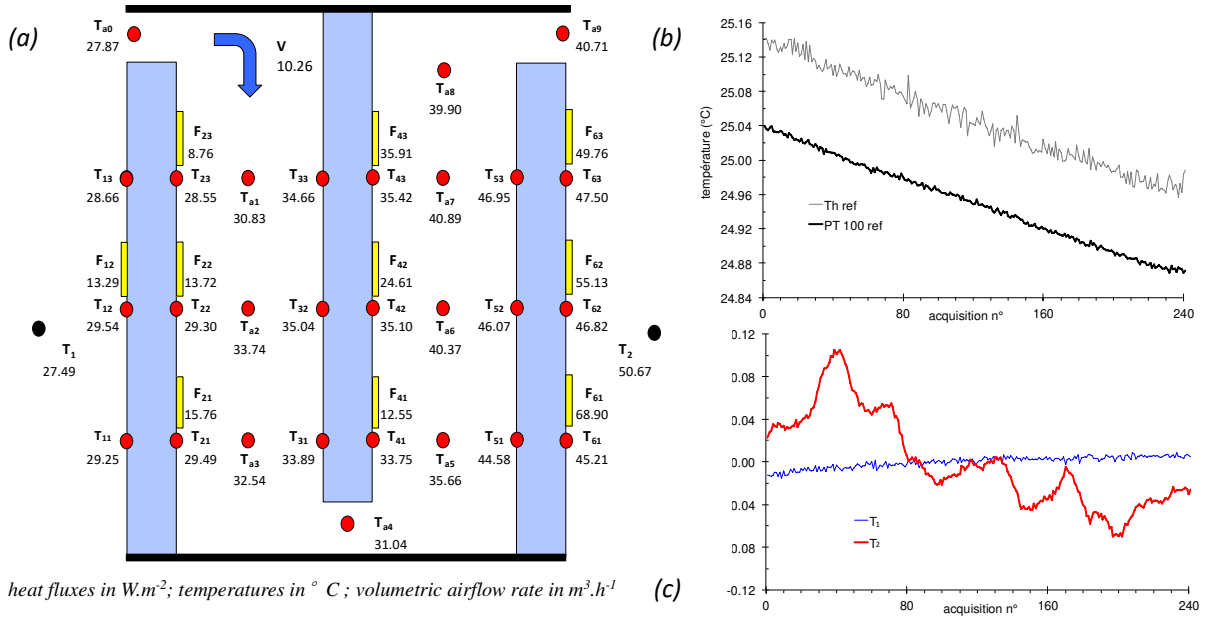

Figure 4: Example of experimental results (Test no. 3): (a) the average measurement for each sensor; (b) temperature evolution in the laboratory, as measured by a thermocouple and a PT-100; (c) temperature fluctuations in both cells

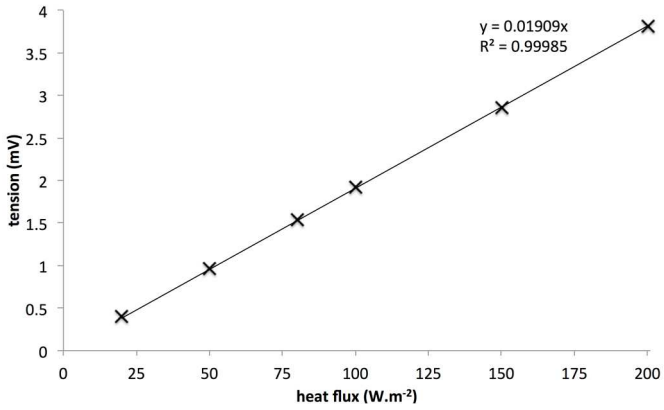

Figure 5: Voltage response to the heat flux for the calibration of fluxmeter F_{61}

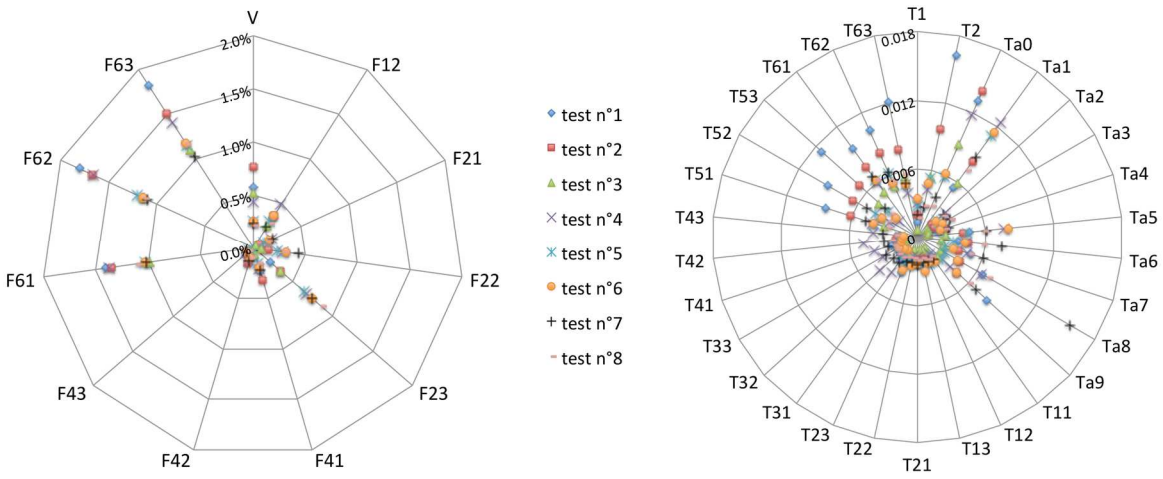

Figure 6: Statistical uncertainties

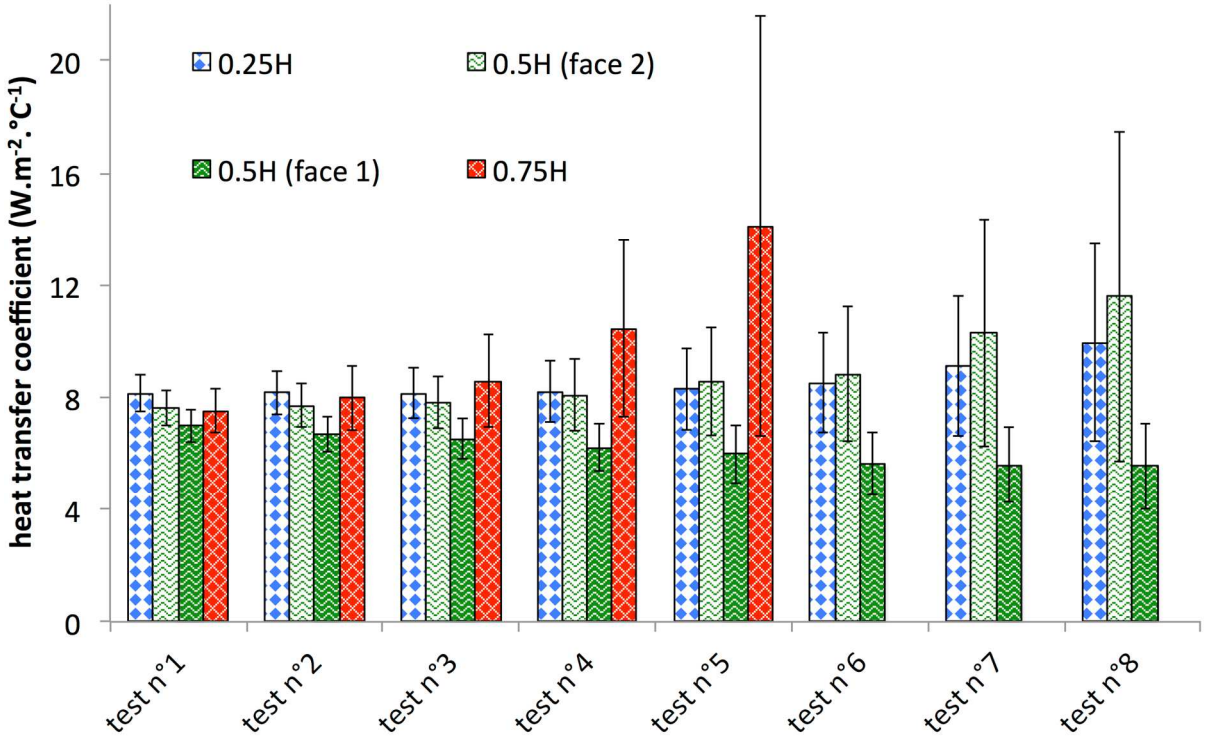

Figure 7: Estimation of the global heat transfer coefficient in the cold cell from temperature measurements (PT-100 T_1, thermocouples T_{12}, T_{21}, T_{22} and T_{23}) and heat fluxes (fluxmeters F_{12}, F_{21}, F_{22} and F_{23})

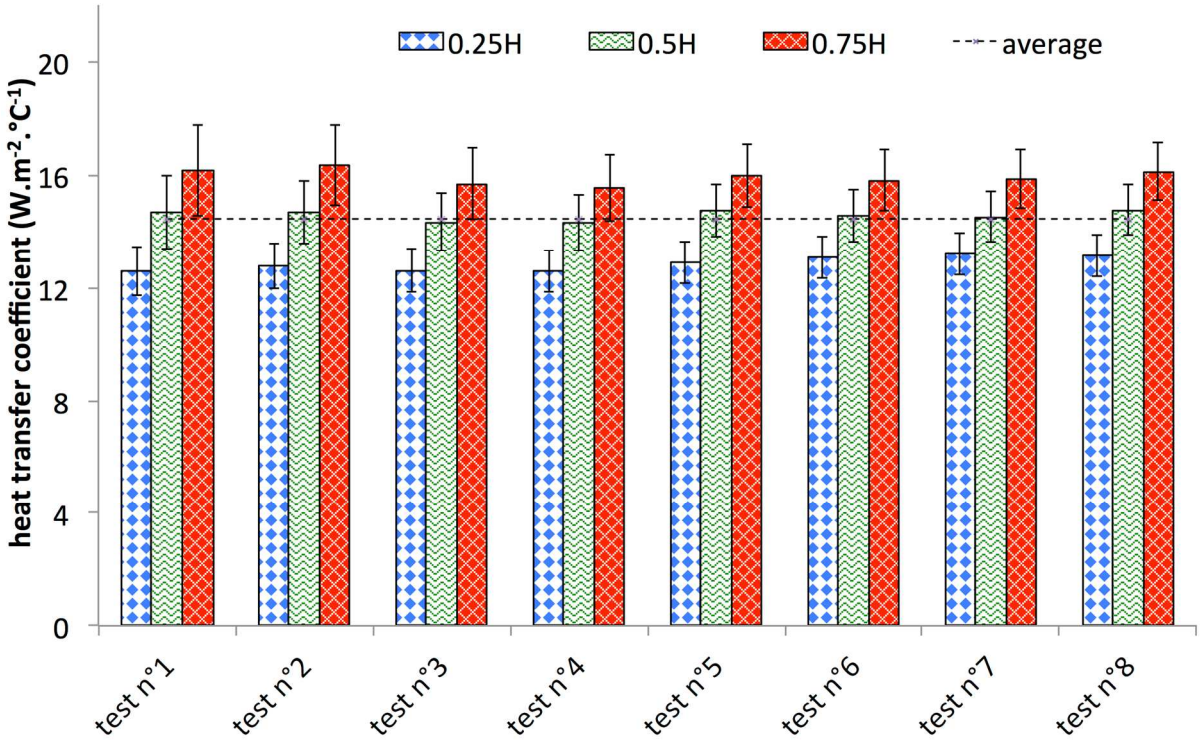

Figure 8: Estimation of the global heat transfer coefficient in the hot cell from temperature measurements (PT-100 T_2, thermocouples T_{61}, T_{62} and T_{63}) and heat fluxes (fluxmeters F_{61}, F_{62} and F_{63})

Model Settings	
Space	2D
Time	Steady
Flow	Laminar
Heat Transfer	Enabled
Radiation	Discrete Ordinate Model

Variable	Dicretization Scheme
Pressure	Second Order
Momentum	Second Order Upwind
Energy	First Order Upwind
Discrete Ordinates	First Order Upwind

Air Properties	
Density	incompressible-ideal-gas
Specific Heat	$1002.737 + 1.2324 \times 10^{-2}.T(K)$
Thermal Conductivity	$2.873 \times 10^{-3} + 7.76 \times 10^{-5}.T(K)$
Dynamic Viscosity	$3.723 \times 10^{-6} + 4.94 \times 10^{-8}.T(K)$

Glass Properties	
Density	$2700\ kg.m^{-3}$
Specific Heat	$840\ J.kg^{-1}.°C^{-1}$
Thermal Conductivity	$1\ W.m^{-1}.°C^{-1}$

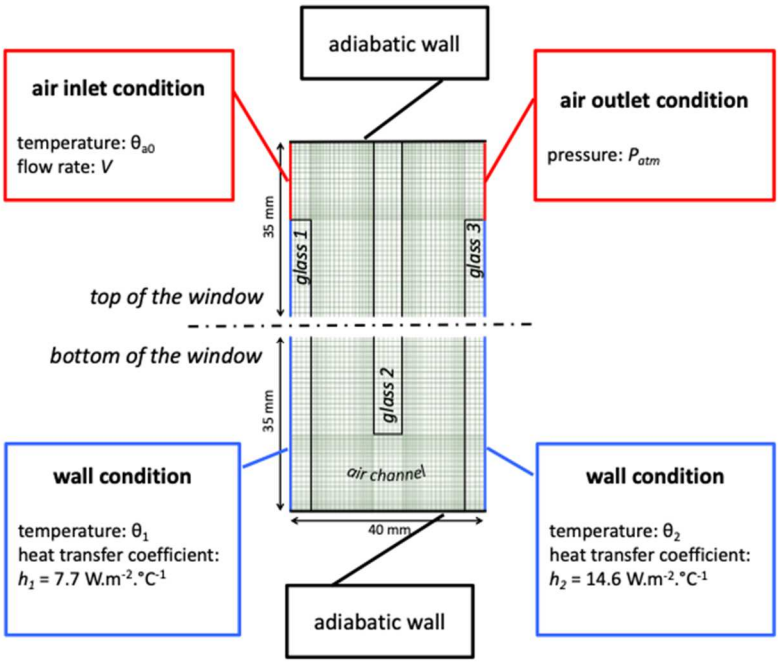

Figure 9: Properties and boundary conditions of the CFD model

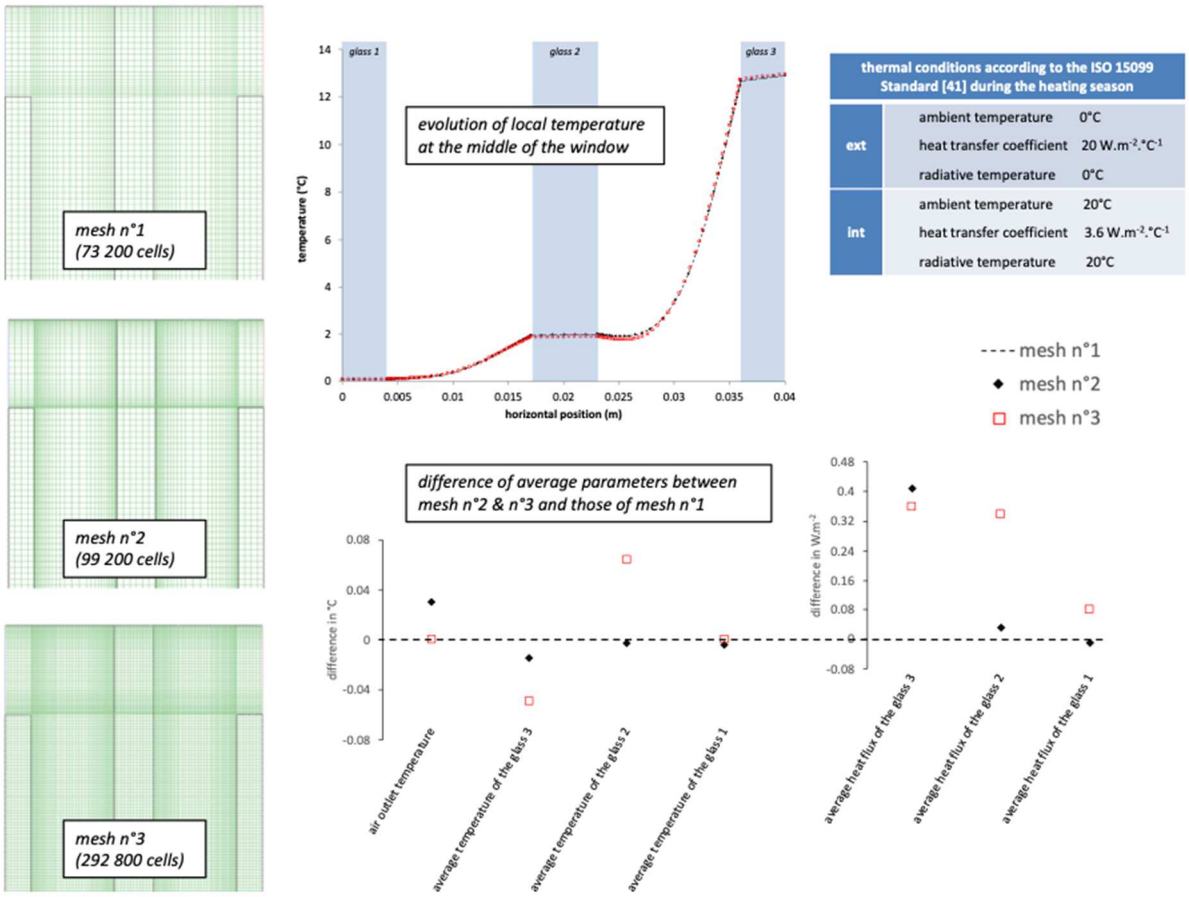

Figure 10: Mesh sensitivity study

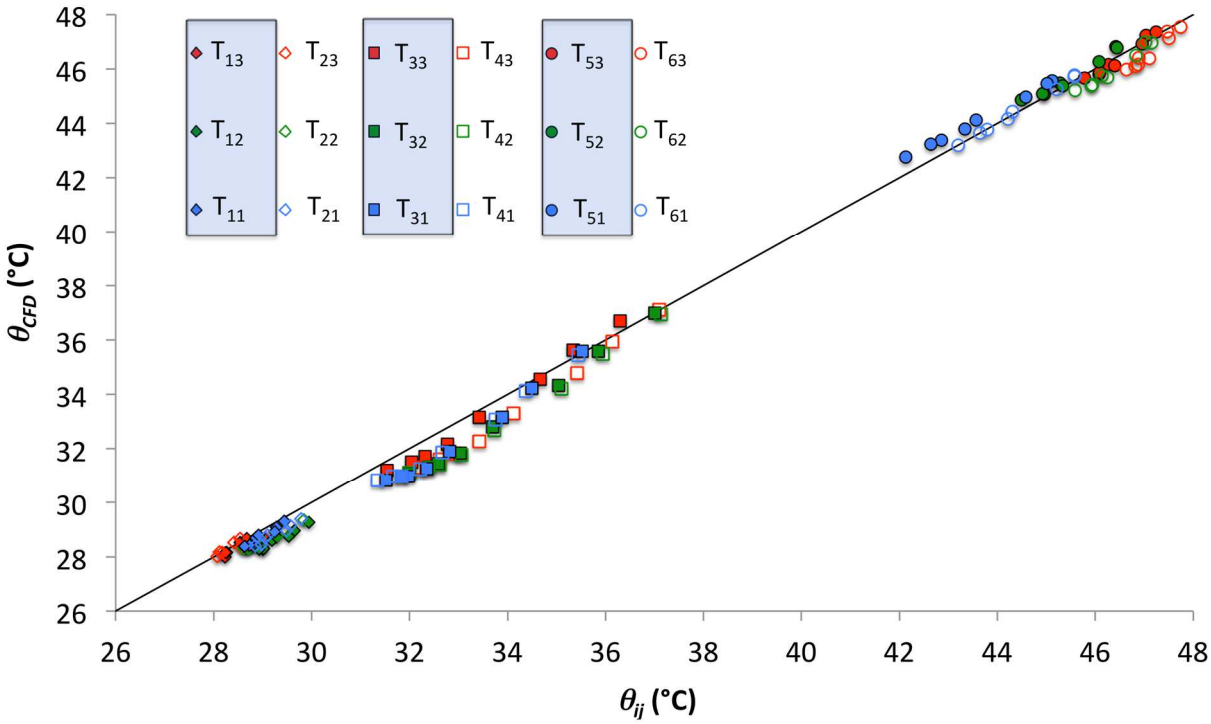

Figure 11: Comparison of temperature estimations from experiments and numerical simulations

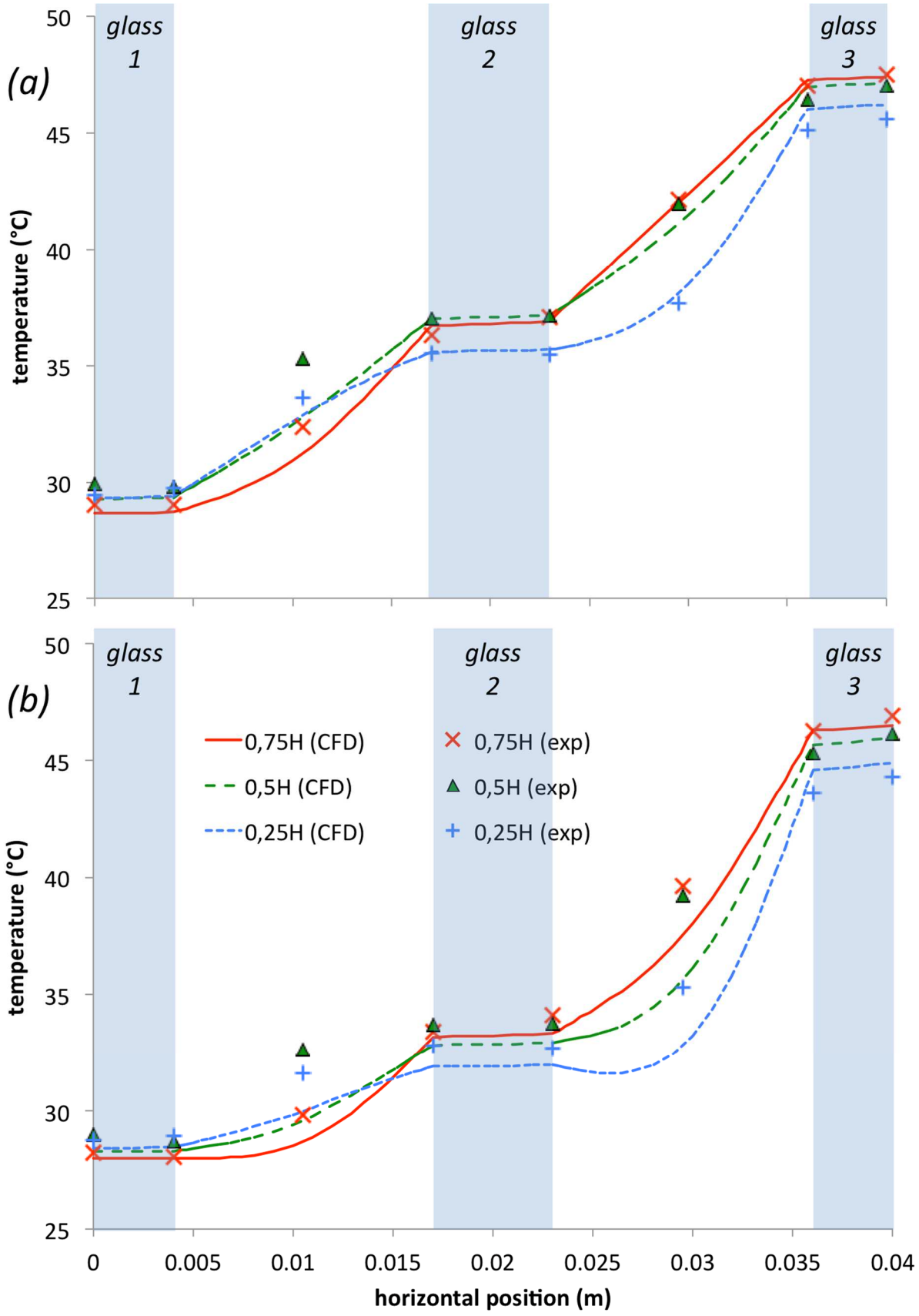

Figure 12: Evolution of temperature in the horizontal sections performed at: 4.99 $m^3.h^{-1}$ (a) and 13.60 $m^3.h^{-1}$ (b)

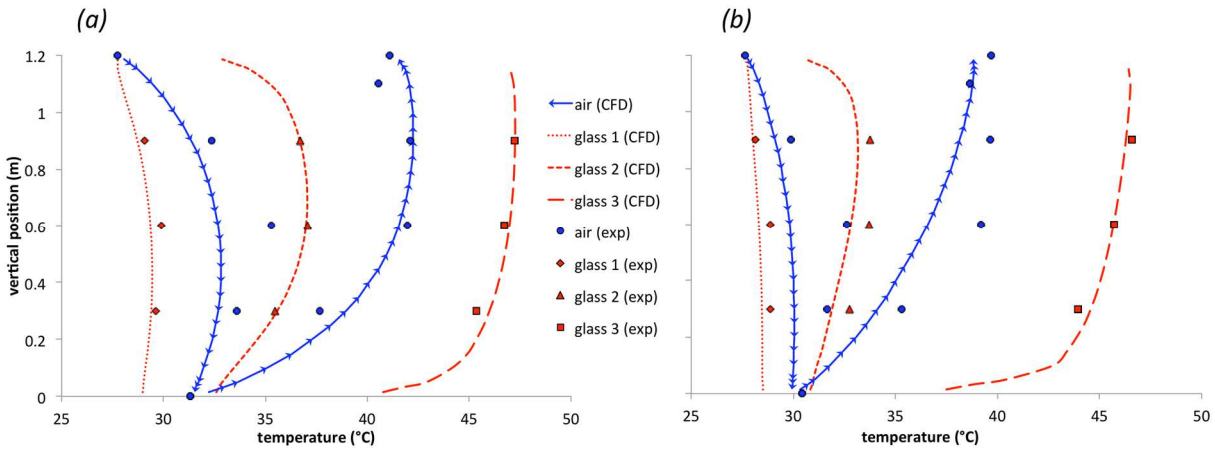

Figure 13: Evolution in both glass and air temperatures vs. window height performed at: 4.99 $m^3.h^{-1}$ (a) and 13.60 $m^3.h^{-1}$ (b)

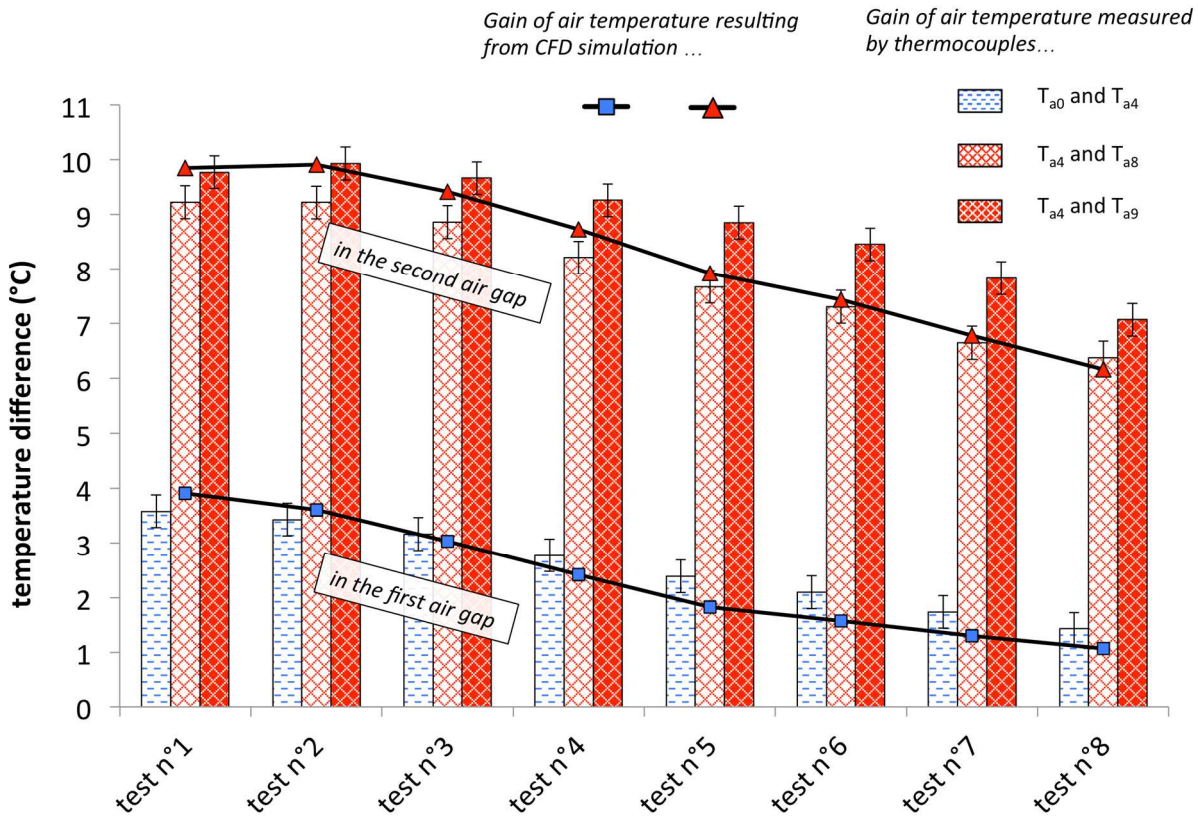

Figure 14: Air temperature increase in the two cavities for each test

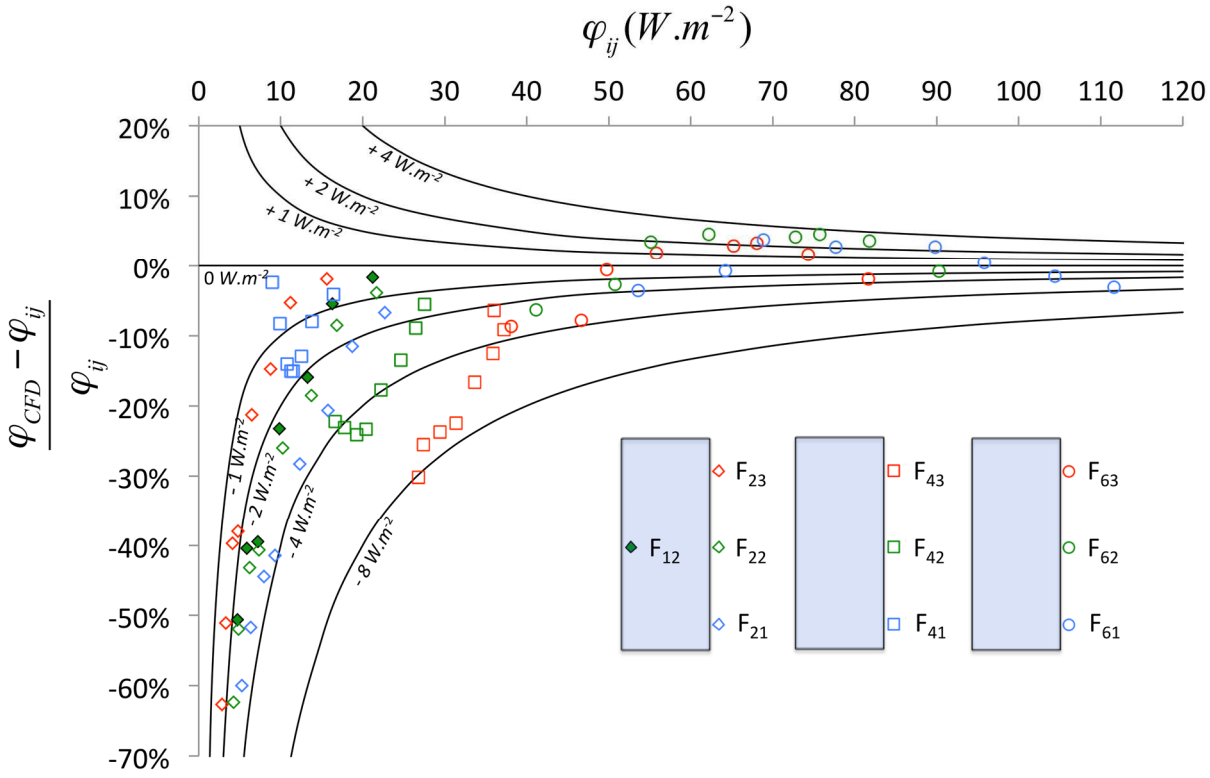

Figure 15: Comparison of heat flux estimations from experiments and numerical simulations

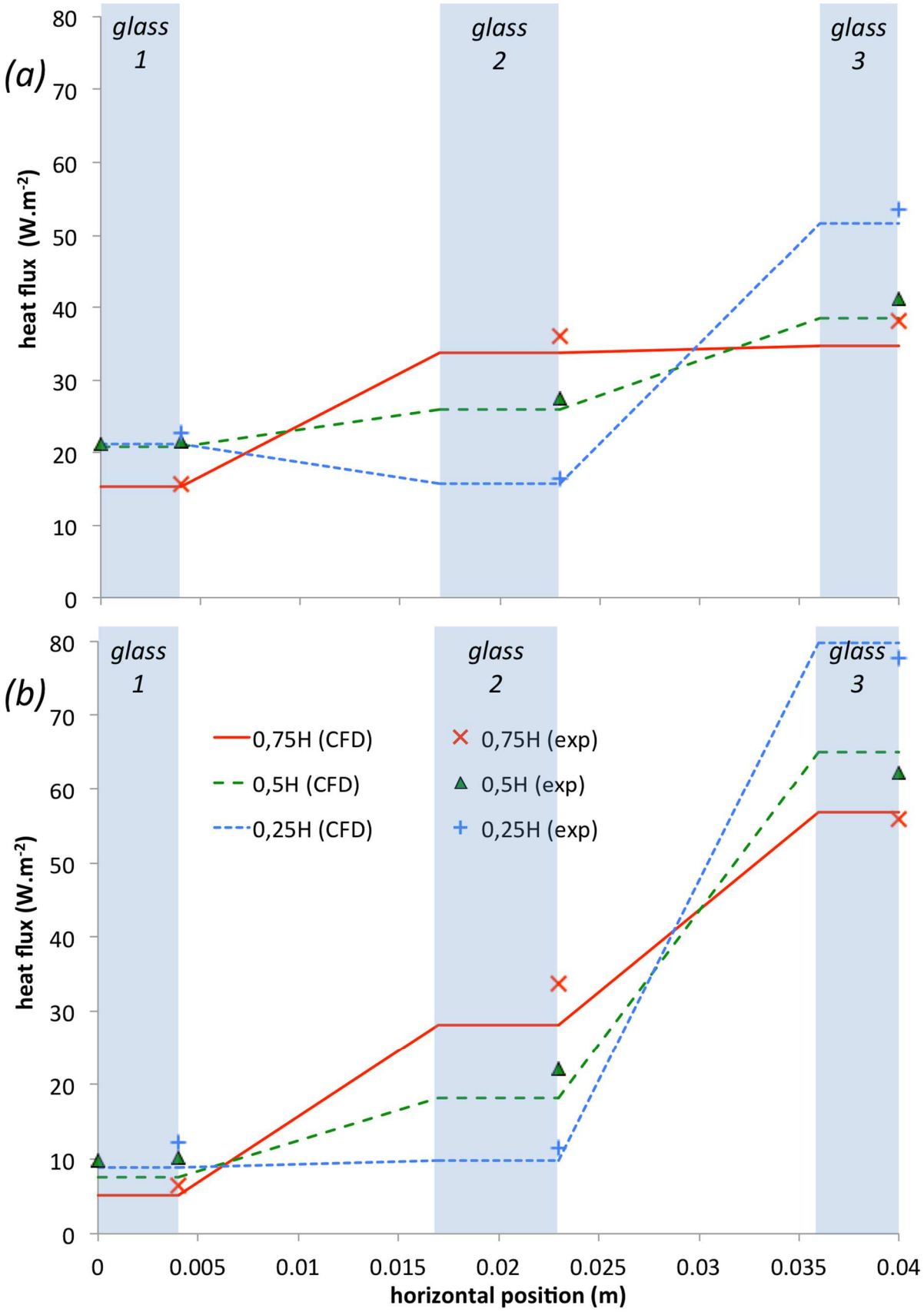

Figure 16: Evolution in heat fluxes in horizontal sections performed at: 4.99 $m^3.h^{-1}$ (a) and 13.60 $m^3.h^{-1}$ (b)

Table 1
Overview of laboratory experiments

test n°	test duration (h)	time interval between acquisitions (s)	acquisitions numbers per sensor	measured volumetric airflow rate ($m^3.h^{-1}$)	measured temperature in laboratory (°C)	measured temperature in cold cell (°C)	measured temperature in hot cell (°C)	temperature difference between the two test cells (°C)
1	1	30	120	5.0	23.41	26.91	49.82	22.91
2	1	30	120	7.7	24.64	27.20	50.60	23.40
3	2	30	240	10.3	24.95	27.49	50.67	23.18
4	1	30	120	13.6	25.22	27.42	50.48	23.06
5	2	30	240	18.8	25.31	27.81	51.18	23.37
6	1	20	180	21.4	26.45	27.88	51.12	23.24
7	2	30	240	25.8	26.83	28.34	51.56	23.32
8	1	20	180	30.7	26.85	28.55	51.70	23.15

Table 2
Uncertainty value applied for each sensor

Measurement of...	Uncertainties	
temperature by thermocouple	ω_{th}	0.2°C
temperature by PT-100	ω_{pt}	0.02°C
heat flux by fluxmeter	ω_f / φ	5 %
airflow rate by anemometer	ω_a / V	2 %